Role of the Seasonal Cycle in the Subduction Rates of Upper–Southern Ocean Waters

Eun Young Kwon*

Department of Atmospheric and Oceanic Sciences, University of California, Los Angeles, Los Angeles, California

Stephanie M. Downes

Research School of Earth Sciences, and ARC Centre of Excellence for Climate System Science, The Australian National University, Acton, Australian Capital Territory, Australia

Jorge L. Sarmiento

Atmospheric and Oceanic Sciences Program, Princeton University, Princeton, New Jersey

Riccardo Farneti

Earth System Physics Section, ICTP, Trieste, Italy

Curtis Deutsch

Department of Atmospheric and Oceanic Sciences, University of California, Los Angeles, Los Angeles, California

ABSTRACT

A kinematic approach is used to diagnose the subduction rates of upper–Southern Ocean waters across seasonally migrating density outcrops at the base of the mixed layer. From an Eulerian viewpoint, the term representing the temporal change in the mixed layer depth (which is labeled as the temporal induction in this study; i.e., $S_{temp} = \partial h/\partial t$ where h is the mixed layer thickness, and t is time) vanishes over several annual cycles. Following seasonally migrating density outcrops, however, the temporal induction is attributed partly to the temporal change in the mixed layer thickness averaged over a density outcrop following its seasonally varying position and partly to the lateral movement of the outcrop position intersecting the sloping mixed layer base. Neither the temporal induction following an outcrop nor its integral over the outcrop area vanishes over several annual cycles. Instead, the *seasonal eddy subduction*, which arises primarily because of the subannual correlations between the seasonal cycles of the mixed layer depth and the outcrop area, explains the key mechanism by which mode waters are transferred from the mixed layer to the underlying pycnocline. The time-mean exchange rate of waters across the base of the mixed layer is substantially different from the exchange rate of waters across the fixed winter mixed layer base in mode water density classes. Nearly 40% of the newly formed Southern Ocean mode waters appear to be diapycnally transformed within the seasonal pycnocline before either being subducted into the main pycnocline or entrained back to the mixed layer through lighter density classes.

* Current affiliation: Research Institute of Oceanography, Seoul National University, Seoul, South Korea.

Corresponding author address: Eun Young Kwon, Research Institute of Oceanography, Seoul National University, 1 Gwanak-ro, Gwanak-gu, Seoul 151-742, South Korea.
E-mail: ekwon76@snu.ac.kr

1. Introduction

The upper ocean is ventilated by subduction of water masses in mid- and high latitudes where pycnocline water masses outcrop at the surface. Observations show that water mass properties within the main pycnocline are very similar to the properties in the winter mixed layer of the outcrop regions (e.g., Iselin 1939). Based on

this finding, Stommel (1979) suggested that mixed layer waters are transferred to the main pycnocline at the end of winter when the main pycnocline is directly in contact with the mixed layer. Modeling studies (Woods 1985; Williams et al. 1995) deploying Lagrangian particles in the mixed layer indeed show that subduction occurs preferentially from late winter to early spring when the deep mixed layer shoals rapidly because of seasonal buoyancy forcing. The subducted upper water masses spread along isopycnals zonally and meridionally (Sloyan and Rintoul 2001; Koch-Larrouy et al. 2010), transporting heat, freshwater, nutrients, and dissolved gases from the sea surface to the ocean's interior (e.g., Toggweiler et al. 1989; Sarmiento et al. 2004; Sabine et al. 2004).

One of the most widely used approaches for diagnosing the subduction rate of upper water masses is the kinematic approach of Cushman-Roisin (1987). The instantaneous subduction/obduction rate S is defined as the vertical velocity of a parcel of water relative to the base of the instantaneous mixed layer, $z = -h$, expressed as

$$S = \frac{D[z - (-h)]}{Dt} = w_h + \frac{Dh}{Dt} = w_h + \frac{\partial h}{\partial t} + U_h \cdot \nabla h, \quad (1)$$

where h is the thickness of the mixed layer and is a function of geographic location and time, and w_h and U_h [$U_h = (u_h, v_h)$] are the Eulerian vertical and horizontal velocities of a water parcel at the base of the mixed layer, respectively (Cushman-Roisin 1987; Nurser and Marshall 1991); w_h, u_h, and v_h are positive upward, eastward, and northward, respectively. Here positive S represents obduction (upward velocity), and negative S represents subduction (downward velocity); Dh/Dt is the material derivative of the mixed layer thickness following a horizontal movement of a water parcel moving with a velocity of U_h, and takes into account a change in the mixed layer thickness with time in a Lagrangian framework (e.g., Nurser and Marshall 1991, see also Fig. 1b). This approach based on the instantaneous subduction rate allows us to estimate the volume of water transferred across the base of the mixed layer per unit area per unit time. A spatially integrated instantaneous subduction rate gives the volume of water that is exchanged between the mixed layer and the underlying pycnocline per unit time.

A similar approach, later proposed by Marshall et al. (1993), defined the subduction rate to the main pycnocline as the vertical velocity of a parcel of water relative to a time-invariant winter mixed layer base, $z = -H$, expressed as

$$S_H = \frac{D[z - (-H)]}{Dt} = w_H + \frac{DH}{Dt} = w_H + U_H \cdot \nabla H, \quad (2)$$
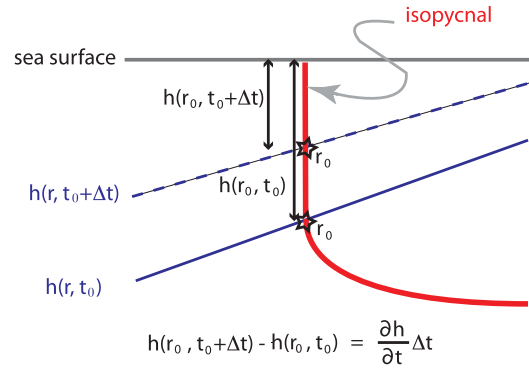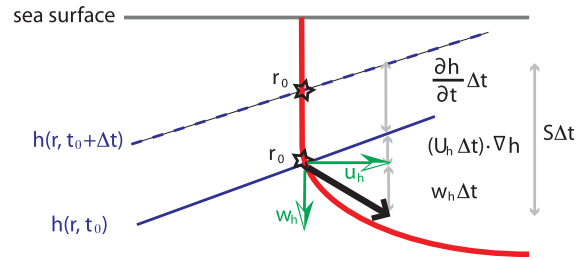

FIG. 1. Schematics illustrating the subduction rate in an Eulerian frame of reference. (a) An ideal ocean at rest where the mixed layer depth shoals from the solid line $h(r, t_0)$ to the dashed line $h(r, t_0 + \Delta t)$. The subduction rate evaluated at a fixed lateral location of r_0 becomes $S = \partial h/\partial t$. (b) A more realistic case where a water parcel moves with a velocity of (U_h, w_h) while the mixed layer base shoals from the solid line to the dashed line. The subduction rate in this case becomes $S = \partial h/\partial t + U_h \cdot \nabla h + w_h$. The schematic is adapted from Nurser and Marshall (1991).

where H is the winter mixed layer thickness and is a function of geographic location only; w_H and U_H [$U_H = (u_H, v_H)$] are the Eulerian vertical and horizontal velocities of a water parcel at the base of the winter mixed layer. Because the spatial distribution of H is held constant with time (Marshall et al. 1993), the annual mean subduction rate into the main pycnocline can simply be obtained by

$$S_{ann} = \overline{S_H} = \overline{w_H} + \overline{U_H} \cdot \nabla H, \quad (3)$$

where the overbar denotes an annual average taken with a geographic location fixed. An integral of Eq. (3) over a time-invariant winter outcrop area gives the net volume exchange rate of waters across the base of the winter mixed layer. Equation (3) is also equivalent to the integral of instantaneous subduction rate over the effective subduction period that winter mixed layer waters are irreversibly transferred into the main pycnocline

(Marshall et al. 1993; Williams et al. 1995). The effective subduction period in mid- and high latitudes was found to be about 1 month starting from the end of winter, in support of the Stommel's mixed layer demon hypothesis (Stommel 1979; Marshall et al. 1993; Williams et al. 1995).

Modeling studies that employed both of the kinematic approaches of Eqs. (1) and (2) found substantial differences in the two estimates (Hazeleger and Drijfhout 2000; Da Costa et al. 2005; Nishikawa et al. 2010); within a given density range, the time-mean volume transport obtained from Eq. (1) gives a net volume flux of mode waters entering the seasonal and main pycnocline that is substantially greater than that estimated from Eq. (2) into the main pycnocline. The fundamental difference between the Marshall et al.'s subduction rate and the original Cushman–Roisin's subduction rate is the different definitions used in the two equations. When the main pycnocline is capped by the seasonal pycnocline, Eq. (2) gives the exchange rate of water between the seasonal pycnocline and the underlying main pycnocline (Qiu and Huang 1995), whereas Eq. (1) always tracks the exchange rate of water between the mixed layer and the seasonal or main pycnocline. Thus, the difference in the time-mean subduction rates obtained based on the two definitions can be attributed to diapycnal processes that may occur within the seasonal pycnocline (Nishikawa et al. 2010).

In this paper, we revisit the instantaneous subduction rate, Eq. (1), in a quasi-Lagrangian framework that tracks the seasonally migrating water mass outcrops. This new framework enables us to explore the role of seasonal stratification of the upper ocean and associated migration of density outcrops in determining the annual mean subduction rates of upper–Southern Ocean waters. In the Southern Ocean, mode and intermediate waters are formed within and north of the Antarctic Circumpolar Current (ACC) (e.g., McCartney 1977; Hanawa and Talley 2001; Dong et al. 2008), where deep winter convection drives the deepest mixed layer depths of ~500 m (Dong et al. 2008). As the seasonal buoyancy forcing restratifies the upper ocean, the mixed layer shoals to ~50 m in summer, and at the same time, the density outcrop migrates toward the South Pole (Fig. 2). This seasonal migration of isopycnals results in a change of the area over which upper water masses outcrop at the base of the mixed layer. In general, the outcrop areas expand toward the equator during cooling period and contracts toward the South Pole during heating period. As will be shown in this study, it is the subannual correlations between the outcrop area and the rate of shoaling/deepening of the mixed layer that give rise to the time-mean net volume subduction of mode waters out of the mixed layer. By comparing the estimates

obtained using Eqs. (1) and (2), we also show that a portion of the subducted water undergoes diapycnal transformation within the seasonal pycnocline before either being subducted into the main pycnocline or entrained back to the mixed layer.

The most important term representing the seasonal cycle of the upper ocean dynamics is $\partial h/\partial t$ in Eq. (1). For a discussion purpose, we label the $\partial h/\partial t$ term as the *temporal induction* S_{temp}, along the lines of the lateral induction labeled for $U_h \cdot \nabla h$ (Marshall et al. 1993). We note that the temporal induction has a physical significance when the lateral induction term is also taken into consideration (i.e., $Dh/Dt = \partial h/\partial t + U_h \cdot \nabla h$) and that these two terms are not separable in the kinematic approach deploying Lagrangian particles (e.g., Williams et al. 1995). Thus, Dh/Dt as a whole may be referred to as the lateral induction of water beneath the temporally changing mixed layer base (e.g., Woods 1985), analogous to the ''lateral induction'' beneath the time-invariant winter mixed layer base in Marshall et al. (1993) (i.e., $DH/Dt \equiv U_H \cdot \nabla H$). Nonetheless, we find the $\partial h/\partial t$ term useful in explaining the volume exchange rate of mode waters across the base of the mixed layer and hence discuss this term in great detail. It is straightforward that the temporal average of $\partial h/\partial t$ vanishes when it is evaluated at a fixed geographic location of an Eulerian frame of reference. Following a seasonally migrating density outcrop, however, the annual mean of $\partial h/\partial t$ does not vanish for the following two reasons.

(i) Applying the chain rule, the temporal induction in the Eulerian coordinate can be rewritten as,

$$S_{\text{temp}} = \left.\frac{\partial h}{\partial t}\right|_r = \left.\frac{\partial h}{\partial t}\right|_\sigma - \left.\frac{\partial r}{\partial t}\right|_\sigma \cdot \left.\frac{\partial h}{\partial r}\right|_t = \left.\frac{\partial h}{\partial t}\right|_\sigma - U_h^\sigma \cdot \nabla h,$$

$$(4)$$

where $\partial h/\partial t|_r$ is the Eulerian partial derivative of the mixed layer thickness with respect to time holding a geographic location $r = (x, y)$ constant; this Eulerian partial derivative is denoted as $\partial h/\partial t$ in Eq. (1) (we omit ''$|_r$'' in the Eulerian derivative for convenience); $\partial h/\partial t|_\sigma$ is the partial derivative of the mixed layer thickness with respect to time holding density σ constant (i.e., following a density outcrop); $\partial r/\partial t|_\sigma$ is the lateral velocity of an outcrop position, denoted as U_h^σ (see Fig. 3 for illustrations); $\partial h/\partial t|_t$ is the lateral gradient of the mixed layer thickness ∇h.

Now we consider an annual average of Eq. (4). To make a distinction between an Eulerian averaging and an averaging following a density outcrop, we use a notation of $\overline{\partial h/\partial t}^\sigma$ for the isopycnal averaging while
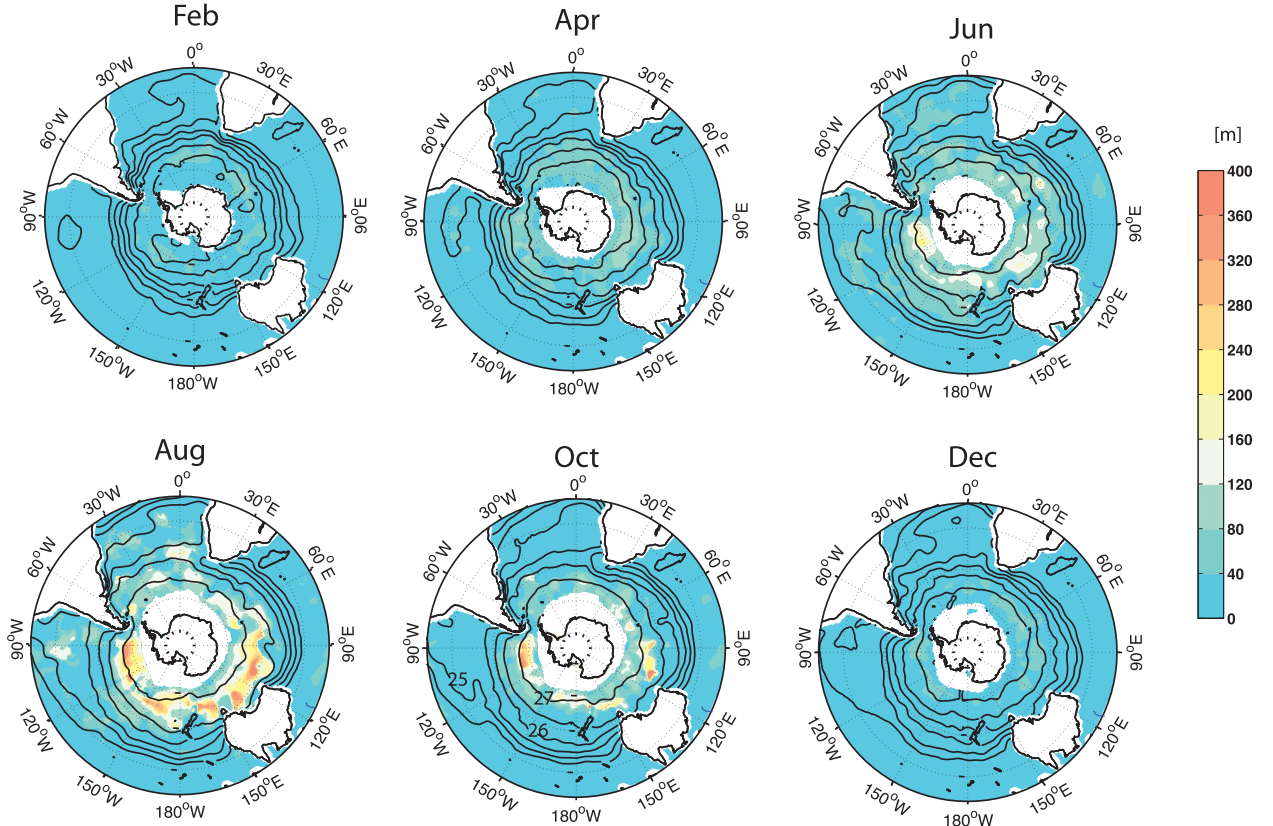
FIG. 2. The monthly climatology of the mixed layer thickness and potential density at the base of the mixed layer, as obtained from the *World Ocean Atlas 2009* (Locarnini et al. 2010; Antonov et al. 2010). The color shade represents the monthly mean mixed layer thickness (m). Black solid lines are the isolines of potential density at the base of the mixed layer. The potential density σ is evaluated at the sea surface. The southernmost contour corresponds to $\sigma = 27.0$ ($\rho = 1027.0$ kg m^{-3}) and the northernmost contour corresponds to $\sigma = 24.5$ ($\rho = 1024.5$ kg m^{-3}). The contour interval is $\Delta\sigma = 0.5$. The areal extent of sea ice around Antarctica is shown in white shading in the maps, and is based on the monthly climatology data of sea ice concentrations (Reynolds et al. 2002). The ocean domain south of 10°S is shown.

the Eulerian averaging is denoted as $\overline{\partial h/\partial t} \equiv \overline{\partial h/\partial t}^r$ for convenience. The Eulerian average of the temporal induction (i.e., $\overline{\partial h/\partial t}$) vanishes over repeating annual cycles such that $\overline{\partial h/\partial t}|_\sigma$ balances $\overline{U_h^\sigma \cdot \nabla h}$. In a quasi-Lagrangian framework following an outcrop, on the other hand, $\overline{\partial h/\partial t}|_\sigma^\sigma$ vanishes for the same reason that $\overline{\partial h/\partial t}$ vanishes. In this case, $\overline{\partial h/\partial t}^\sigma$ balances $\overline{-U_h^\sigma \cdot \nabla h}^\sigma$. Because the latter term does not vanish when the seasonal anomalies of U_h^σ and ∇h are correlated, the temporal induction following an outcrop (i.e., $\overline{\partial h/\partial t}^\sigma$) does not necessarily vanish over several annual cycles.

(ii) Following Marshall (1997), an areal integral of the temporal induction averaged over a year, $\overline{M_{\text{temp}}}^\sigma$, can be written as

$$\overline{M_{\text{temp}}}^\sigma = \overline{(S_{\text{temp}} \cdot A)}^\sigma = \overline{S_{\text{temp}}}^\sigma \cdot \overline{A}^\sigma + \overline{(S'_{\text{temp}} \cdot A')}^\sigma,$$

(5)

where the annual mean is obtained following a density outcrop, the prime denotes the deviation from the annual mean (i.e., the seasonal perturbation), and A is an outcrop area. As will be shown in this paper, the eddy term $\overline{(S'_{\text{temp}} \cdot A')}^\sigma$ dominates the net volume subduction, particularly in Subantarctic Mode Water (SAMW) density classes. In other words, the outcrop area of mode waters tends to be larger during the subduction period than does during the obduction period. This results in net annual mean volume transport out of the mixed layer, a significant portion of which will then be subducted into the main pycnocline.

The net transfer resulting from the subannual correlations between subduction rates and outcrop areas will be referred to as the *seasonal eddy subduction* in this study, in an attempt to emphasize the role of the seasonal cycle. We note that the "eddy subduction" has already been formulated and interpreted in terms of roles
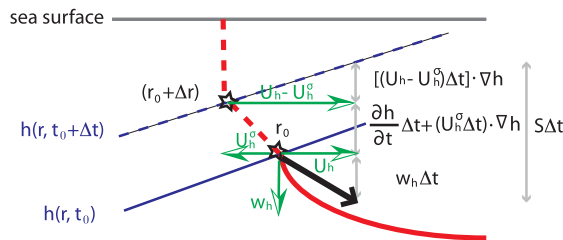
(a)
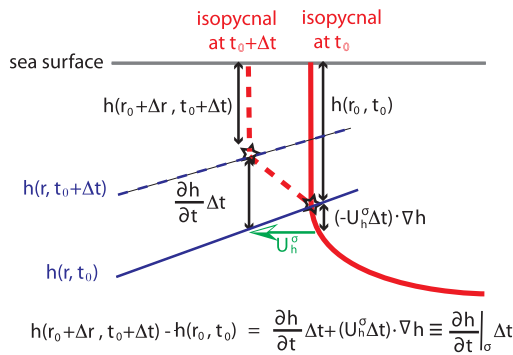
(b)

FIG. 3. Schematics illustrating the subduction rate in a quasi-Lagrangican framework following a migrating density outcrop position. (a) An ideal ocean at rest where the mixed layer depth shoals from the solid line $h(r, t_0)$ to the dashed line $h(r, t_0 + \Delta t)$ while the lateral position of the outcrop moves from r_0 to $r_0 + \Delta r$. The subduction rate evaluated following the movement of the outcrop position becomes $S = \partial h / \partial t$. The *temporal induction* $S_{\text{temp}} = \partial h / \partial t$ consists of the component caused by the temporal change in the mixed layer thickness evaluated following the outcrop position $S_{\text{temp}}^t = [h(r_0 + \Delta r, t_0 + \Delta t) - h(r_0, t_0)]/\Delta t = \partial h / \partial t + U_h^\sigma \nabla h \equiv \partial h / \partial t|_\sigma$ and the isopycnal lateral induction $S_{\text{temp}}^{xy} = -U_h^\sigma \nabla h$ caused by the lateral movement of the outcrop position intersecting the sloping mixed layer base. (b) A more realistic case where a water parcel moves with a velocity of (U_h, w_h) while the mixed layer base shoals and the outcrop position moves. The subduction rate in this case becomes $S = \partial h / \partial t|_\sigma + (U_h|_\sigma) \cdot \nabla h + w_h \equiv (\partial h / \partial t + U_h^\sigma \cdot \nabla h) + (U_h - U_h^\sigma) \cdot \nabla h + w_h = \partial h / \partial t + U_h \cdot \nabla h + w_h$. See section 2 for details.

of mesoscale eddies in Marshall (1997). Although an important progress was made in the previous work, we feel that the role of the seasonal cycle in the annual mean formation and subduction rates of upper–Southern Ocean waters deserves more attention. Our seasonal eddy subduction does not necessarily involve mesoscale "eddy" activity. Rather, this arises because of seasonal perturbations. We will show that the seasonal cycle and mesoscale eddies conspire to enhance the net subduction of mode waters in the Southern Ocean.

This paper is organized as follows. In section 2, we revisit the kinematic approach for diagnosing the instantaneous subduction rate, such that each term in Eq. (1) can be reinterpreted in a quasi-Lagrangian framework that follows seasonally migrating density outcrops. In section 3, we describe a numerical model and methods employed in this study. In section 4, we explore the role of the seasonal cycle in determining the time-mean subduction rates of upper–Southern Ocean waters. Finally, we summarize this paper in section 5.

2. Revisiting the kinematic approach

We revisit the kinematic approach for diagnosing the instantaneous subduction rate, formulated in Eq. (1). Section 2a offers a review of Eq. (1) in an Eulerian viewpoint. In section 2b, we reinterpret Eq. (1) in a quasi-Lagrangian framework following a varying density outcrop position. In section 2c, we review the expression for the instantaneous volume subduction, which is an area-integral of the subduction rate.

a. A diagnostic of subduction rate evaluated at a fixed geographic location

For simplicity, we first consider a water parcel in an idealized ocean at rest. We assume that the mixed layer moves up and down while the lateral isopycnal position remains fixed with time (Fig. 1a). The vector $r_0 = (x_0, y_0)$ is the horizontal location of the intersection between the mixed layer base and the isopycnal surface at time $t = t_0$. The depth at which the mixed layer base intersects the isopycnal surface changes from $z = -h(r_0, t_0)$ at time $t = t_0$ to $z = -h(r_0, t_0 + \Delta t)$ at time $t = t_0 + \Delta t$. From an Eulerian perspective at the location $r = r_0$, the temporal induction S_{temp} is

$$S_{\text{temp}} = \lim_{\Delta t \to 0} \frac{h(r_0, t_0 + \Delta t) - h(r_0, t_0)}{\Delta t} = \frac{\partial h}{\partial t}, \quad (6)$$

which becomes negative (subduction) when the mixed layer shoals and positive (obduction) when the mixed layer deepens.

Now we consider a water parcel moving with a velocity (U_h, w_h) at the location $r = r_0$ and the depth $z = -h(r_0, t_0)$ while the mixed layer shoals from $h(r_0, t_0)$ to $h(r_0, t_0 + \Delta t)$ (Fig. 1b). The subduction rate caused by the vertical movement of the water parcel becomes w_h, and the subduction rate caused by the lateral movement of the water parcel intersecting the sloping mixed layer base becomes $U_h \cdot \nabla h$. Taken together, the full equation for the subduction rate of a water parcel evaluated at a fixed location becomes Eq. (1), that is

$$S = \frac{Dh}{Dt} + w_h = \frac{\partial h}{\partial t} + U_h \cdot \nabla h + w_h.$$

b. A diagnostic of subduction rate evaluated following a migrating density outcrop

In this section, we are concerned with the subduction rate relative to the base of the mixed layer, evaluated following a varying outcrop position of density σ. For simplicity, we first consider a water parcel in an idealized ocean at rest. The mixed layer base moves up and down while the density isoline migrates horizontally within the seasonal pycnocline with time. Figure 3 depicts the case where the mixed layer shallows while the isopycnal surface shifts southward (poleward) with time. Over the time interval of Δt, the horizontal location of the intersection between the mixed layer base and the isopycnal surface moves from $r = r_0$ to $r = r_0 + \Delta r$, and the mixed layer thickness shallows from $h(r_0, t_0)$ to $h(r_0 + \Delta r, t_0 + \Delta t)$, holding density σ constant. In this case, the temporal induction S_{temp} constitutes (i) the subducton rate S_{temp}^t caused by the temporal change in the mixed layer thickness holding density σ constant and (ii) the subduction rate S_{temp}^{xy} caused by the lateral velocity of a density outcrop position intersecting the sloping mixed layer base, where the lateral velocity of a density outcrop position is denoted as $U_h^\sigma = \Delta r / \Delta t|_\sigma$ (Fig. 3a).

(i) S_{temp}^t can be expressed as

$$S_{temp}^t = \lim_{\Delta t \to 0} \frac{h(r_0 + \Delta r, t_0 + \Delta t) - h(r_0, t_0)}{\Delta t} = \frac{\partial h}{\partial t}\bigg|_\sigma,$$
(7)

where $(\partial h/\partial t)|_\sigma$ represents a partial derivative of mixed layer thickness with respect to time, holding density σ constant. Applying the chain rule [see Eq. (4)], Eq. (7) can be rewritten as

$$S_{temp}^t = \frac{\partial h}{\partial t}\bigg|_\sigma = \frac{\partial h}{\partial t} + U_h^\sigma \cdot \nabla h,$$
(8)

where U_h^σ is positive when the isopycnal migrates northward with time and negative when the isopycnal migrates southward.

(ii) S_{temp}^{xy} is

$$S_{temp}^{xy} = -U_h^\sigma \cdot \nabla h,$$
(9)

which represents the lateral induction caused by the velocity of the reference point. The negative sign is needed because r_0 is moving with a velocity of $-U_h^\sigma$ relative to $r_0 + \Delta r$. Equation (9) is combined with Eq. (8) to yield the temporal induction S_{temp}

$$S_{temp} = S_{temp}^t + S_{temp}^{xy}$$
$$= \left(\frac{\partial h}{\partial t} + U_h^\sigma \cdot \nabla h\right) + (-U_h^\sigma \cdot \nabla h) = \frac{\partial h}{\partial t}, \quad (10)$$

which is identical to the Eulerian derivative of the mixed layer thickness with respect to time $\partial h/\partial t$.

Now we consider a parcel of water moving with a velocity of (U_h, w_h) at the location $r = r_0$ and the depth $z = -h(r_0, t_0)$ while the mixed layer thickness shoals from $h(r_0, t_0)$ to $h(r_0 + \Delta r, t_0 + \Delta t)$ (Fig. 3b). The resulting full equation for the instantaneous subduction rate relative to the base of the mixed layer, evaluated following a migrating density outcrop, becomes

$$S = \frac{Dh}{Dt} + w_h$$
$$= \left(\frac{\partial h}{\partial t} + U_h^\sigma \cdot \nabla h\right) + (U_h - U_h^\sigma) \cdot \nabla h + w_h$$
$$= \frac{\partial h}{\partial t}\bigg|_\sigma + (U_h|_\sigma) \cdot \nabla h + w_h, \quad (11)$$

where $U_h|_\sigma = U_h - U_h^\sigma$ is the effective lateral velocity of a water parcel relative to a migrating density outcrop. Dh/Dt is the material derivative of the mixed layer thickness following a lateral movement of a water parcel and can be interpreted in terms of the change in the mixed layer thickness in a Lagrangian frame of reference from the migrating density outcrop perspective. Note that Eq. (11) is identical to Eq. (1) except that the term Dh/Dt is repartitioned.

c. A diagnostic of volume flux across a migrating density outcrop

Now, we move onto an expression for diagnosing the volume flux of water across the base of the mixed layer. From Eq. (11), an instantaneous volume transport across the base of the mixed layer becomes

$$M(\sigma_1 \le \sigma < \sigma_2, t)$$
$$= \int_{A(\sigma_1 \le \sigma < \sigma_2, t)} \left[\frac{\partial h}{\partial t}\bigg|_\sigma + (U_h|_\sigma) \cdot \nabla h + w_h\right] dA, \quad (12)$$

where $M(\sigma_1 \le \sigma \le \sigma_2, t)$ (m^3 s^{-1}) is the volume flux of water transferred across the base of the mixed layer, integrated over a density interval $\sigma_1 \le \sigma \le \sigma_2$ at time t; $A(\sigma_1 \le \sigma \le \sigma_2, t)$ is the area over which waters of the density range outcrop at the base of the mixed layer. Operationally, Eq. (12) can be computed by binning the area-integrated subduction rate of Eq. (1) into density
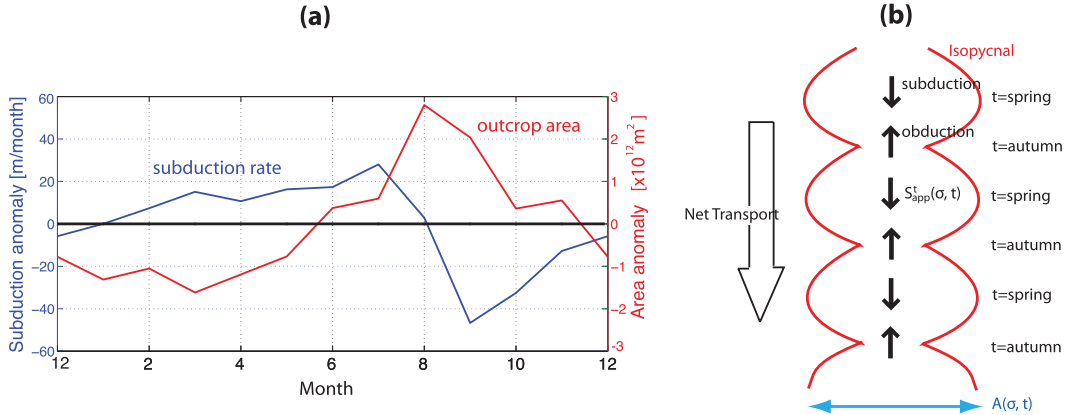
(a)   **(b)**

FIG. 4. (a) *The World Ocean Atlas 2009* monthly variations of the temporal change in the mixed layer thickness evaluated following the outcrop S^t_{temp} and the outcrop area anomaly A', averaged over a density bin of $\sigma = 26.7$. The anomaly is defined as a deviation from the annual mean. Positive rate represents obduction and negative represents subduction. The subannual correlations between S^t_{temp} and A' lead to a nonzero value of $\overline{(S^t_{\text{temp}} \cdot A')}^\sigma = 4\,\text{Sv}$, although $\overline{(S^t_{\text{temp}})}^\sigma = 0\,\text{Sv}$ and $\overline{A'}^\sigma = 0\,\text{m}^2$. (b) A cartoon illustrating the *seasonal eddy subduction* resulting from the subannual correlations between the subduction/obduction rate $S^t_{\text{temp}}(\sigma, t)$ and outcrop area $A(\sigma, t)$. Both $S^t_{\text{temp}}(\sigma, t)$ and $A(\sigma, t)$ are functions of density σ and time t. Subduction occurs in early spring when the mixed layer shallows and obduction occurs in autumn when the mixed layer deepens. The outcrop area is relatively larger during the subduction period than during the obduction period, leading to net downward volume transport. This schematic is adapted from Marshall (1997).

intervals. The time-averaged volume of waters subducted below the mixed layer becomes

$$\overline{M(\sigma_1 \leq \sigma < \sigma_2)}^\sigma$$
$$= \frac{1}{T} \int_t \int_{A(\sigma_1 \leq \sigma < \sigma_2, t)} \left(\left. \frac{\partial h}{\partial t} \right|_\sigma + (U_h|_\sigma) \cdot \nabla h + w_h \right) dA\, dt, \quad (13)$$

where T is the time period considered for the average.

In what follows, we focus on the time-averaged volume transport across the base of the mixed layer, caused by the temporal induction evaluated following a density outcrop position. As is the case for the temporal induction, the corresponding volume flux can be divided into two: (i) the temporal change in the mixed layer thickness integrated over a migrating density outcrop and (ii) the volume transport driven by the outcrop movement intersecting the sloping mixed layer base:

$$\overline{M_{\text{temp}}(\sigma_1 \leq \sigma < \sigma_2)}^\sigma = \overline{M^t_{\text{temp}}(\sigma_1 \leq \sigma < \sigma_2)}^\sigma + \overline{M^{xy}_{\text{temp}}(\sigma_1 \leq \sigma < \sigma_2)}^\sigma, \quad (14)$$

where

$$\overline{M^t_{\text{temp}}(\sigma_1 \leq \sigma < \sigma_2)}^\sigma = \frac{1}{T} \int_t \int_{A(\sigma_1 \leq \sigma < \sigma_2, t)} \left(\left. \frac{\partial h}{\partial t} \right|_\sigma \right) dA\, dt,$$

and

$$\overline{M^{xy}_{\text{temp}}(\sigma_1 \leq \sigma < \sigma_2)}^\sigma = \frac{1}{T} \int_t \int_{A(\sigma_1 \leq \sigma < \sigma_2, t)} (-U^\sigma_h \cdot \nabla h)\, dA\, dt.$$

As will be illustrated in the next section, both components ($\overline{M^t_{\text{temp}}}^\sigma$ and $\overline{M^{xy}_{\text{temp}}}^\sigma$) make significant contributions to the net volume transport into the pycnocline. In the Southern Ocean, the outcrop areas of mode and intermediate waters increase as the outcrops move toward the equator from summer to winter, and decrease as the outcrops move toward the South Pole from winter to summer (Figs. 2 and 4a). At the same time, the subduction rate ($S^t_{\text{temp}} = \partial h/\partial t|_\sigma$) caused by the temporal change in the mixed layer thickness following density σ also changes seasonally, that is, subduction during the spring when the mixed layer shallows and obduction during the autumn when the mixed layer deepens (Fig. 4). The seasonal cycle of S^t_{temp} is highly correlated with the seasonal cycle of A. This subannual correlations result in a nonzero annual mean volume flux (i.e., $\overline{M^t_{\text{temp}}}^\sigma \neq 0$) even though the annual mean subduction rate is zero (i.e., $\overline{S^t_{\text{temp}}}^\sigma = \overline{\partial h/\partial t|_\sigma}^\sigma = 0$). In a simple expression,

$$\overline{M^t_{\text{temp}}}^\sigma = \overline{(S^t_{\text{temp}} \cdot A)}^\sigma = \overline{S^t_{\text{temp}}}^\sigma \cdot \overline{A}^\sigma + \overline{[(S^t_{\text{temp}})' \cdot A']}^\sigma, \quad (15)$$

which is similar to Eq. (5). Net volume transport from the mixed layer into the pycnocline occurs because the
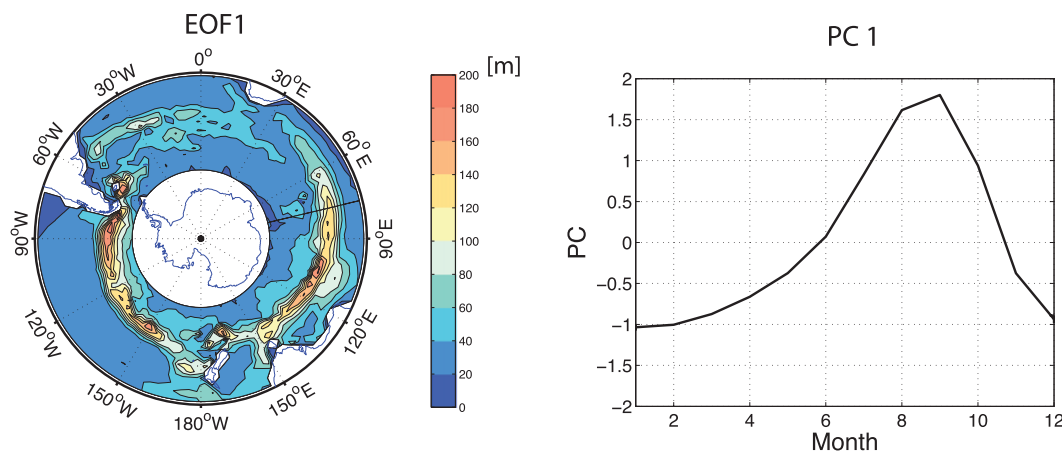
FIG. 5. The leading empirical orthogonal function (EOF) pattern of the monthly mean mixed layer thickness, and the corresponding principle component (PC) time series. This mode accounts for 85% of the total variance of the mixed layer thickness, and represents the seasonal cycle of the mixed layer thickness. A 20-yr simulation is used to compute the EOF. The monthly mean of the PC time series is shown here.

average outcrop area is relatively larger during the subduction period than during the obduction period. The concept of the downward transport of $\overline{M^t_{\text{temp}}}^\sigma$ is analogous to the eddy bolus transport or the eddy thickness transport (e.g., Marshall and Radko 2003; Marshall 1997; see also Fig. 4b), which refers to the transport caused by the subgrid-scale correlations between the velocity of water and the thickness of isopycnal. The eddy contribution of the temporal induction, $\overline{[(S^t_{\text{temp}})' \cdot A']}^\sigma$ is the key component of the seasonal eddy subduction rate represented by $\overline{(S' \cdot A')}^\sigma$.

3. Model and methods

a. The CM2.4 Model and the water mass definitions

We use the Climate Model, version 2.4 (CM2.4), developed by the National Oceanic and Atmospheric Administration (NOAA)'s Geophysical Fluid Dynamics Laboratory (Farneti et al. 2010; Farneti and Delworth 2010). The ocean model is the depth-based vertical coordinate Modular Ocean Model, version 4p1 (Griffies 2009), with a horizontal resolution of approximately $0.25° \times 0.25°$ and a vertical resolution for the 50 depth levels ranging from 10 m near the surface to 200 m near the bottom. There is no parameterization of eddy-induced transport and background diffusivity in the model. The ocean model is coupled with a thermo-dynamical–dynamical sea ice model and an atmospheric model without flux adjustments. The atmospheric component is the 1° horizontal resolution model of Delworth et al. (2006). The model is integrated for a few centuries with a constant 1990-radiative forcing. We use the model solutions for the year 171–180 in which model

solutions are saved with three different temporal samplings (i.e., 10-year monthly climatology, monthly mean and 5-day mean).

We consider a model domain of the Southern Hemisphere and the outcrop density range of $\sigma = 25.0-27.2$ (i.e., $\rho = 1025.0-1027.2$ kg m^{-3}) where the potential density σ is referenced to the sea surface. The density range is subdivided into 22 density bins with an interval of $\Delta\sigma = 0.1$. As identified in Downes et al. (2011) and will be shown in section 4d, the simulated potential density is biased toward lighter density by $\Delta\sigma = 0.2-0.4$ compared to observations. Thus, the model density range corresponds to approximately $\sigma = 25.4-27.6$ for the real ocean. By restricting the outcrops of interest to those ventilating the open ocean pycnocline, we avoid the influence of sea ice on the water mass formation (see Fig. 2). The mixed layer depth is determined by the depth criterion of $|\sigma_h - \sigma_s| = 0.03$ kg m^{-3}, where σ_s is the potential density at the surface and σ_h is the potential density at the base of the mixed layer (de Boyer Montégut et al. 2004). The simulated seasonal cycle of the mixed layer thickness agrees reasonably well with that of the observed mixed layer thickness (cf. Fig. 5 with Fig. 2 in Sallée et al. 2010); the model captures the phase and amplitude of the observed seasonal cycle of the Southern Ocean mixed layer thickness reasonably well. Following previous studies (McCartney 1977; Hanawa and Talley 2001; Dong et al. 2008), we refer to the water mass formed by deep winter convection (i.e., the density range with the pronounced seasonal cycle in the mixed layer thickness) as Subantarctic Mode Water (SAMW; the $26.0 \leq \sigma < 26.8$ density range for the CM2.4 model). In this study, surrounding density ranges heavier and lighter than SAMW are referred to as Antarctic

TABLE 1. Water mass definitions in this study.

Acronyms	Full name	Density range in CM2.4	Density range in ECCO2
STMW	Subtropical Mode Water	$25.0 \leq \sigma < 26.0$	$25.2 \leq \sigma < 26.4$
SAMW	Subantarctic Mode Water	$26.0 \leq \sigma < 26.8$	$26.4 \leq \sigma < 27.1$
AAIW	Antarctic Intermediate Water	$26.8 \leq \sigma < 27.2$	$27.1 \leq \sigma < 27.6$

Intermediate Water (AAIW; $26.8 \leq \sigma < 27.2$) and Sub-tropical Mode Water (STMW; $25.0 \leq \sigma < 26.0$), respectively (see Table 1 for summary). We note that the regional differences of mode and intermediate water densities are not resolved in this study.

b. Decomposition of the subduction diagnostics

To elucidate the mechanisms by which upper–Southern Ocean waters are transferred to the pycnocline, we separate four components contributing to the net subduction rate: (i) the temporal induction (S_{temp}^t) caused by the temporal change in the mixed layer thickness evaluated following a density outcrop; (ii) the temporal induction (S_{temp}^{xy}) caused by the lateral movement of an outcrop position intersecting the sloping mixed layer base; (iii) the lateral induction (S^{xy}) due to the lateral velocity of water intersecting the sloping mixed layer base; and (iv) the subduction (S^z) due to the vertical velocity of water at the base of the mixed layer (See Table 2 for summary). Thus Eq. (11) is decomposed into the four components as

$$S = S_{temp}^t + S_{temp}^{xy} + S^{xy} + S^z$$
$$= \left.\frac{\partial h}{\partial t}\right|_\sigma + (-U_h^\sigma) \cdot \nabla h + U_h \cdot \nabla h + w_h. \quad (16)$$

Likewise, the net volume subduction, Eq. (12), is decomposed as follows:

$$M = M_{temp}^t + M_{temp}^{xy} + M^{xy} + M^z$$
$$= \int_A \left(\left.\frac{\partial h}{\partial t}\right|_\sigma\right) dA + \int_A (-U_h^\sigma \cdot \nabla h) \, dA$$
$$+ \int_A (U_h \cdot \nabla h) \, dA + \int_A (w_h) \, dA. \quad (17)$$

We note that this decomposition of the subduction rate is an intermediate step toward clarifying subduction mechanisms and that each component may not necessarily be physically meaningful. For example, the sum of the three terms $S_{temp}^t + S_{temp}^{xy} + S^{xy}$ corresponds to Dh/Dt in Eq. (1), which represents a change in the mixed layer thickness following a lateral movement of a water parcel in a Lagrangian frame of reference. In a Lagrangian framework following a water parcel, the Dh/Dt term would not be separable. Nevertheless, we find the decomposition useful to show that the seasonal eddy subduction arises primarily because of S_{temp}^t that is correlated with seasonal change in the outcrop area (see section 4). In the following subsection, we describe how we diagnose S_{temp}^t and S_{temp}^{xy} from the model.

c. Decomposition of the temporal induction

The monthly mean temporal induction across the base of the mixed layer, averaged over an outcrop density interval of $\sigma_1 \leq \sigma < \sigma_2$, is diagnosed using Eq. (10), that is,

$$S_{temp}(\sigma_1 \leq \sigma < \sigma_2, t) = \frac{1}{A(\sigma_1 \leq \sigma < \sigma_2, t)} \int_{A(\sigma_1 \leq \sigma < \sigma_2, t)} \left[\frac{h(r, t + \Delta t) - h(r, t - \Delta t)}{2\Delta t}\right] dA, \quad (18)$$

where a centered difference scheme is used to approximate $\partial h/\partial t$. The corresponding volume transport is

$$M_{temp}(\sigma_1 \leq \sigma < \sigma_2, t)$$
$$= \int_{A(\sigma_1 \leq \sigma < \sigma_2, t)} \left[\frac{h(r, t + \Delta t) - h(r, t - \Delta t)}{2\Delta t}\right] dA, \quad (19)$$

which is simply $A(\sigma_1 \leq \sigma < \sigma_2, t) \times S_{temp}(\sigma_1 \leq \sigma < \sigma_2, t)$.

We then decompose the temporal induction S_{temp} into S_{temp}^t and S_{temp}^{xy} as formulated in Eq. (10). Applying

Eqs. (7) and (9) to individual grid points is impractical if not impossible. Thus we first approximate S_{temp}^t as

$$S_{temp}^t(\sigma_1 \leq \sigma < \sigma_2, t)$$
$$\approx \frac{\langle h(\sigma_1 \leq \sigma < \sigma_2, t + \Delta t)\rangle - \langle h(\sigma_1 \leq \sigma < \sigma_2, t - \Delta t)\rangle}{2\Delta t}, \quad (20)$$

where $\langle h(\sigma_1 \leq \sigma < \sigma_2, t)\rangle$ is an area-weighted mixed layer thickness averaged over the density interval of $\sigma_1 \leq \sigma < \sigma_2$ at time t, that is,

TABLE 2. Symbols used in this study. See section 3b for full descriptions. The corresponding volume subduction is denoted as M_{temp}, M^t_{temp}, M^{xy}_{temp}, M^{xy}, and M^z.

Symbol	Description	Mathematical expression
S_{temp}	Temporal induction which is the sum of S^t_{temp} and S^{xy}_{temp}	$\partial h/\partial t$
S^t_{temp}	Change in the mixed layer thickness following outcrops	$\partial h/\partial t|_\sigma$
S^{xy}_{temp}	Lateral move of outcrop intersecting sloping mixed layer base	$(-U^\sigma_h) \cdot \nabla h$
S^{xy}	Lateral advection intersecting the sloping mixed layer base	$U_h \cdot \nabla h$
S^z	The vertical velocity of water at the base of the mixed layer	w_h

$$\langle h(\sigma_1 \le \sigma < \sigma_2, t) \rangle$$

$$\equiv \frac{1}{A(\sigma_1 \le \sigma < \sigma_2, t)} \int_{A(\sigma_1 \le \sigma < \sigma_2, t)} h(r,t)\, dA, \qquad (21)$$

in which an approximation is made such that

$$\frac{1}{A} \int_A \frac{\partial h}{\partial t}\bigg|_\sigma dA \approx \frac{\partial}{\partial t}\bigg|_\sigma \left(\frac{1}{A} \int_A h\, dA \right). \qquad (22)$$

The difference between S_{temp} and S^t_{temp} is regarded as S^{xy}_{temp}, although this method is prone to errors because of the approximation made in Eq. (20). The corresponding volume transport M^t_{temp} and M^{xy}_{temp} are calculated in the same manner as Eq. (19).

4. The subduction rate of upper–Southern Ocean waters

We use the eddy-permitting coupled climate model to explore the subduction rate of upper–Southern Ocean waters. Our focus is to 1) explore the seasonal cycle of the subduction rate and its annual mean; 2) examine the sensitivity of our subduction diagnostics to different temporal samplings of model solutions—in other words, we explore the relative role of the interannual variability and mesoscale eddies in determining the time-mean subduction rate; and 3) compare the metric M based on varying mixed layer thickness with the metric M_H based on the time-invariant winter mixed layer thickness; based on this comparison, we infer diapycnal processes that may occur within the seasonal pycnocline. We shall show that the temporal induction and its seasonal eddy component explain a substantial portion of the annual mean volume transport of mixed layer waters into the pycnocline, particularly in SAMW density classes, and that diapycnal transformation within the seasonal pycnocline highly modulates the subduction rate below the seasonal pycnocline.

We note that the temporal averaging discussed in this section is taken following density outcrops. In fact, an Eulerian average of the volume subduction rate across a time-invariant winter mixed layer base $(\overline{M_H})$ is identical with an isopycnal average of the volume subduction rate across a time-invariant winter mixed layer base $(\overline{M_H}^\sigma)$, because density fields do not change with time at the winter mixed layer base. Therefore, we do not precisely distinguish between the two averaging methods in this section unless it becomes important.

a. Monthly mean subduction rate and its annual mean

The seasonal cycle of the subduction/obduction rate S is dominated by the change in temporal induction $S_{temp} = \partial h/\partial t$ (Fig. 6), consistent with previous studies (e.g., Da Costa et al. 2005; Nishikawa et al. 2010). Subduction occurs in a relatively short period from September to December when the mixed layer shoals rapidly, and obduction occurs from January to August when the mixed layer deepens relatively slowly (Figs. 6b and 6c). Although the seasonal variation in subduction/ obduction is dominated by the term S^t_{temp}, its annual mean $\overline{S^t_{temp}}^\sigma$ vanishes when averaged over the annual cycle (Fig. 7a). However, its corresponding volume subduction $\overline{M^t_{temp}}^\sigma$ does not vanish (Fig. 7b) because the seasonal anomaly of S^t_{temp} is correlated with the seasonal anomaly of outcrop area A (Figs. 6a and 6c). These subannual correlations contribute to significant amount of annual mean volume transport in density ranges centered at $\sigma = {\sim}25.5$ and $\sigma = {\sim}26.4$ (Fig. 7b). In fact, this seasonal eddy subduction provides the single most important driver of the volume transport into the pycnocline in the SAMW density class $\sigma = 26.0-26.8$, and also plays a dominant role in the volume transport of the Subtropical Mode Water (STMW) density class of $\sigma = 25.0-26.0$.

The seasonal amplitudes of the lateral induction S^{xy} and the vertical velocity of water S^z are about an order of magnitude smaller than the seasonal amplitude of the temporal induction S_{temp} (Figs. 6e and 6f). Furthermore, S^{xy} and S^z have less pronounced seasonal variations than S_{temp}, and hence their correlations with the seasonal cycle of the outcrop area are relatively small. Consequently, the contributions of the two components to the seasonal eddy subduction are minor, as evident in the similar patterns between the time-mean velocity plot and the time-mean volume transport plot (Fig. 7).

When annually averaged, the vertical velocity of water plays an important role in the net obduction of Antarctic Intermediate Water (AAIW) density classes ($\sigma = 26.8-27.2$) and in the net subduction of STMW density classes ($\sigma = 25.0-26.0$) (Fig. 7). The vertical velocity of water at the base of the mixed layer is
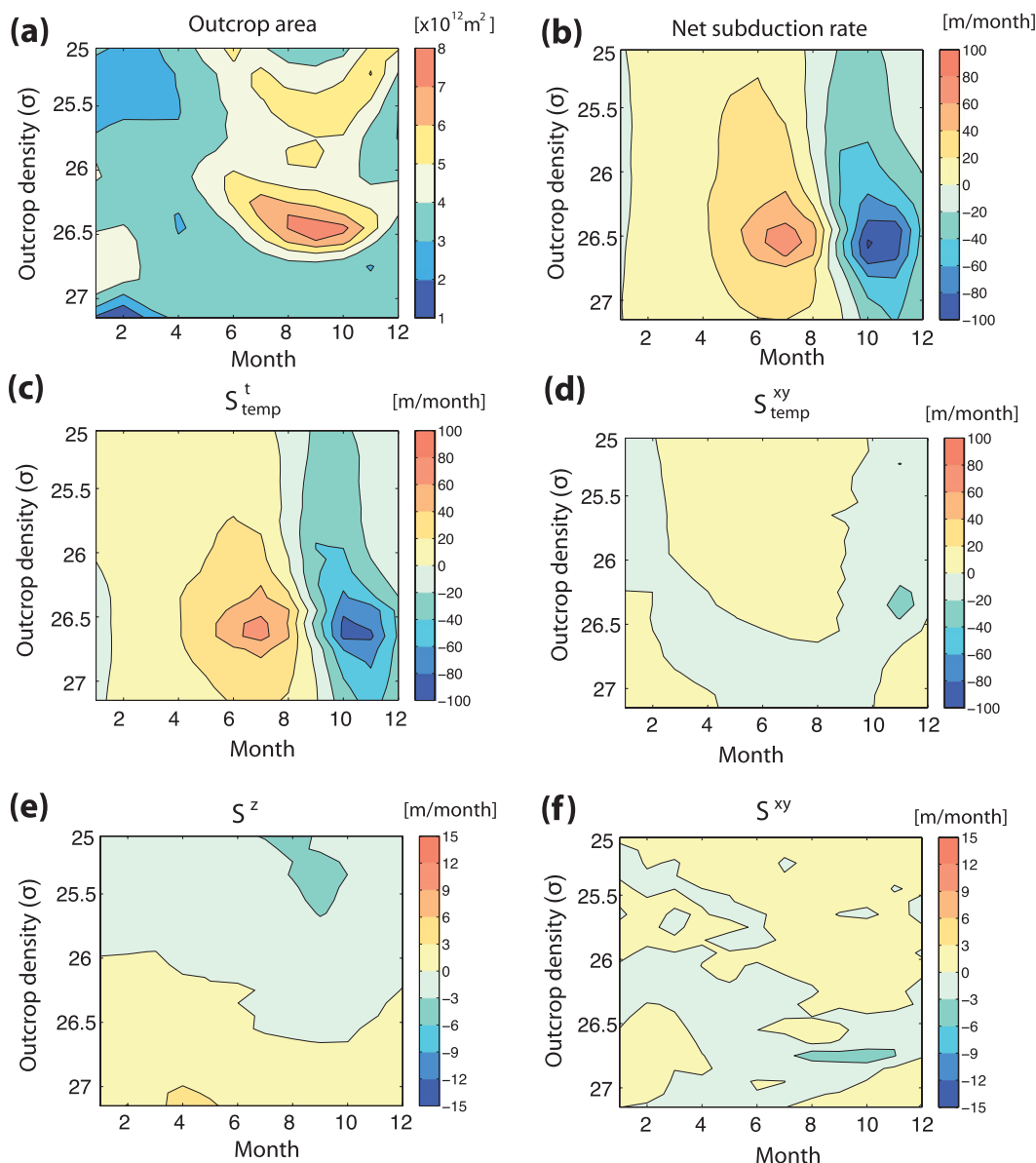
FIG. 6. The 10-yr averages of the monthly mean subduction/obduction rate (m month^{-1}) and outcrop area as functions of month and outcrop density, obtained from the CM2.4 model. (a) The monthly mean outcrop areas. (b) The seasonal cycle of the net subduction/obduction rate S is decomposed into four components: (c) the temporal induction caused by the change in the mixed layer thickness following outcrops $S_{\text{temp}}^{t} = \partial h/\partial t|_{\sigma} = \partial h/\partial t + U_{h}^{\sigma} \cdot \nabla h$, (d) the temporal induction caused by the lateral movement of the outcrop position intersecting the sloping mixed layer base $S_{\text{temp}}^{xy} = -U_{h}^{\sigma} \cdot \nabla h$, (e) the vertical flow at the base of the mixed layer $S^{z} = w_{h}$, and (f) the lateral induction of water $S^{xy} = U_{h} \cdot \nabla h$. Positive values represent obduction, negative values represent subduction.

dominated by the Ekman upwelling south of the Polar Front and downwelling north of the Subantarctic Front. Because the wind-driven vertical transport has a nearly zonal structure determined by the wind stress curl (Sallée et al. 2010), the isopycnally averaged S^{z} and M^{z} show a monotonic tendency with positive values (obduction) in a density range where Ekman upwelling brings pycnocline waters into the mixed layer and

negative values (subduction) in a density range where Ekman downwelling pumps waters down into the pycnocline.

b. Sensitivity to different temporal sampling

In this section, we explore the sensitivity of the subduction diagnostics to three different temporal samplings by comparing the estimate based on the monthly
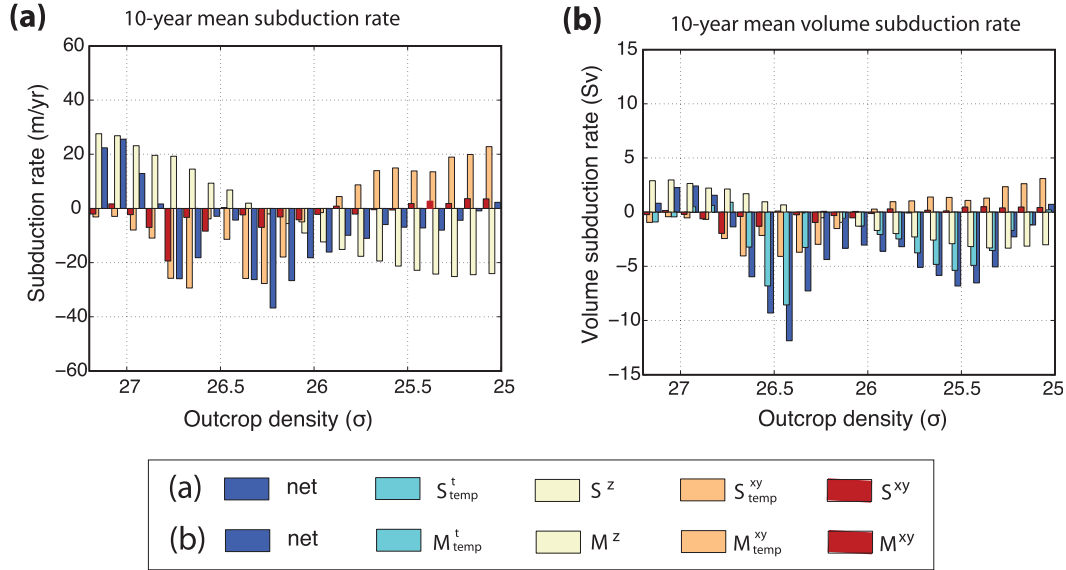
FIG. 7. The 10-yr averages of the annual mean subduction rate (m yr^{-1}) and the volume transport (Sv) across the base of the mixed layer, obtained from the CM2.4 model. (a) The blue bars represent the net subduction/obduction rate S, which is decomposed into contributions from the temporal induction $S^t_{temp} = \partial h/\partial t|_\sigma = \partial h/\partial t + U^\sigma_h \cdot \nabla h$ and $S^{xy}_{temp} = -U^\sigma_h \cdot \nabla h$ (the green and orange bars), the vertical velocity of water at the base of the mixed layer $S^z = w_h$ (the yellow bars), and the lateral induction across the sloping mixed layer base $S^{xy} = U_h \cdot \nabla h$ (the red bars). (b) As in (a), but the net volume subduction M is decomposed into four components M^t_{temp}, M^{xy}_{temp}, M^z, and M^{xy}. Positive values for obduction, negative values for subduction.

mean model solutions (which is presented in the previous section) with cases where 1) we use the 10-yr monthly climatology model solutions and 2) we use the 5-day mean model solutions.

Figure 8 compares the 10-yr-averaged volume subduction, calculated using the three differently sampled model solutions. We find that the net volume transport tends to increase as we increase the temporal resolution of the model output; the overall subduction rates become greater when we use the monthly mean solutions than when we use the monthly climatology means; the subducton rates further increase when we use the 5-day mean solutions than when we use the monthly mean solutions. The most prominent change is found in the outcrop lateral induction M^{xy}_{temp} and the lateral induction M^{xy}, which collectively involve the correlations between the slope of mixed layer base and the lateral *effective* velocity $(U_h - U^\sigma_h)$ of water at the base of the mixed layer. The submonthly time-scale correlations between the lateral effective velocity of water and the horizontal gradient of the mixed layer base causes greater volume transport into the pycnocline in mode water density classes. This is consistent with the previous finding that the high-frequency variability of the upper ocean dynamics (e.g., mesoscale eddies) enhances the net subduction volume fluxes into the pycnocline (Marshall 1997; Hazeleger and Drijfhout 2000; Nishikawa et al.

2010; Follows and Marshall 1994). Nishikawa et al. (2010) found that anticyclonic eddies in the frontal regions tend to deepen the mixed layer and at the same time, induce eddy subduction. It is also possible that the 5-day mean model solutions capture a more precise seasonal cycle than the monthly mean solutions, especially for the rapid shoaling of the mixed layer depth that occurs in spring.

The role of mesoscale and submesoscale processes in determining the net subduction rate of upper–Southern Ocean waters will require further investigations. Nevertheless, our limited sensitivity analysis shows that the seasonal eddy subduction, along with the effect of high-frequency variability, is the primary mechanism by which Southern Ocean mode waters are formed and transferred to the pycnocline.

c. Comparison between the two subduction definitions

We use the monthly climatology model solutions averaged for 10 years to compare between the volume subduction M relative to a varying mixed layer base h and the volume subduction M_H relative to a time-invariant winter mixed layer base H (Figs. 9a and 9c). In other words, we compare the time-mean volume subduction rates obtained from Eqs. (1) and (2). As noted in the introduction, the two estimates are based on two
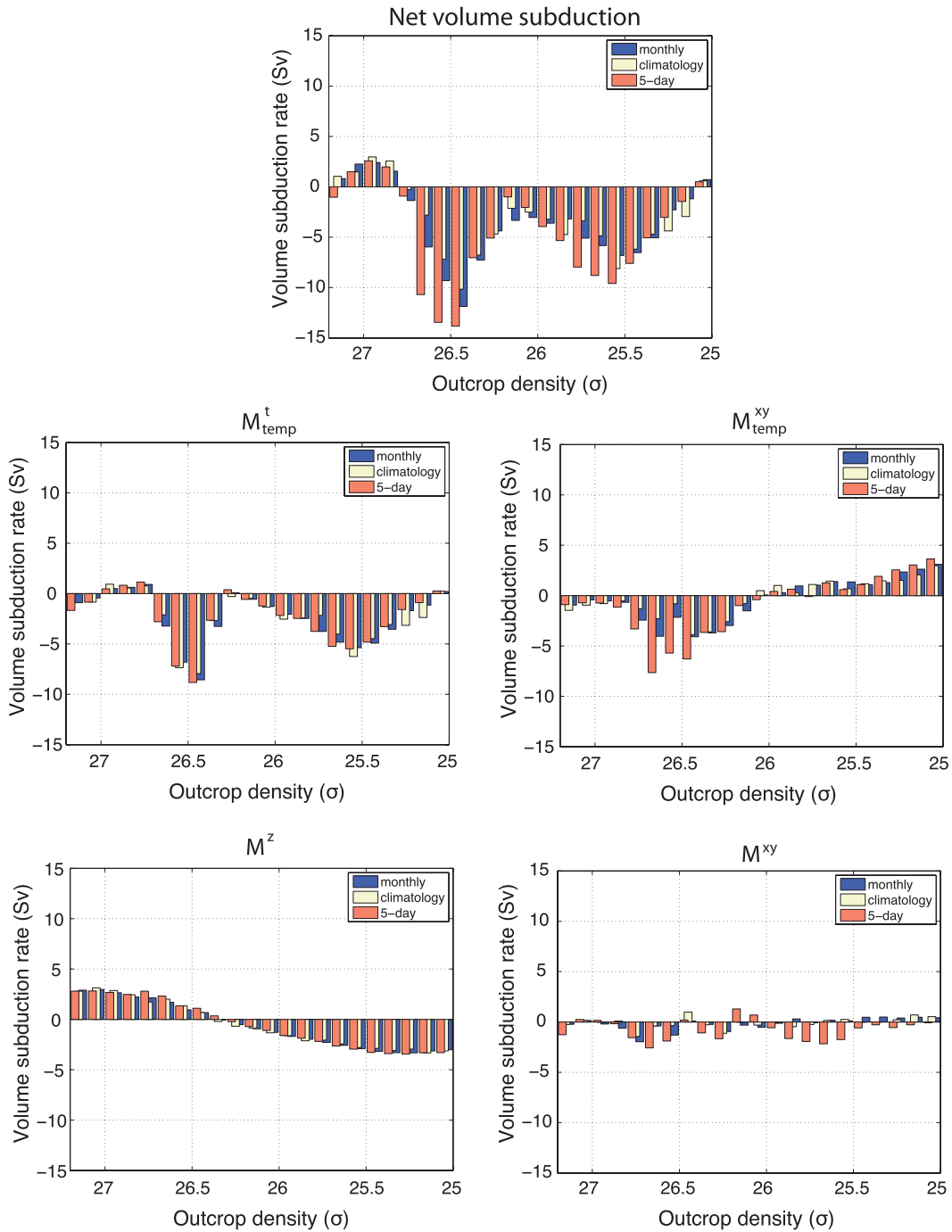
FIG. 8. The 10-yr averages of the annual mean volume fluxes (Sv) across the base of the mixed layer, obtained from the CM2.4 model. The blue bars represent the volume transport calculated using the monthly mean model solutions, which are the same as the blue bars in Fig. 7b. The yellow bars represent the volume transport calculated using the monthly climatology model solutions. The red bars represent the volume transport calculated using the 5-day mean model solutions. (top) The net volume subduction M is decomposed into the contributions from (middle left) $M^t_{\text{temp}} = \int_A (\partial h/\partial t|_\sigma)\, dA = \int_A (\partial h/\partial t + U^\sigma_h \cdot \nabla h)\, dA$, (middle right) $M^{xy}_{\text{temp}} = \int_A (-U^\sigma_h \cdot \nabla h)\, dA$, (bottom left) $M^z = \int_A w_h\, dA$, and (bottom right) $M^{xy} = \int_A (U_h \cdot \nabla h)\, dA$. Positive for obduction, negative for subduction.

Relative to varying mixed layer base

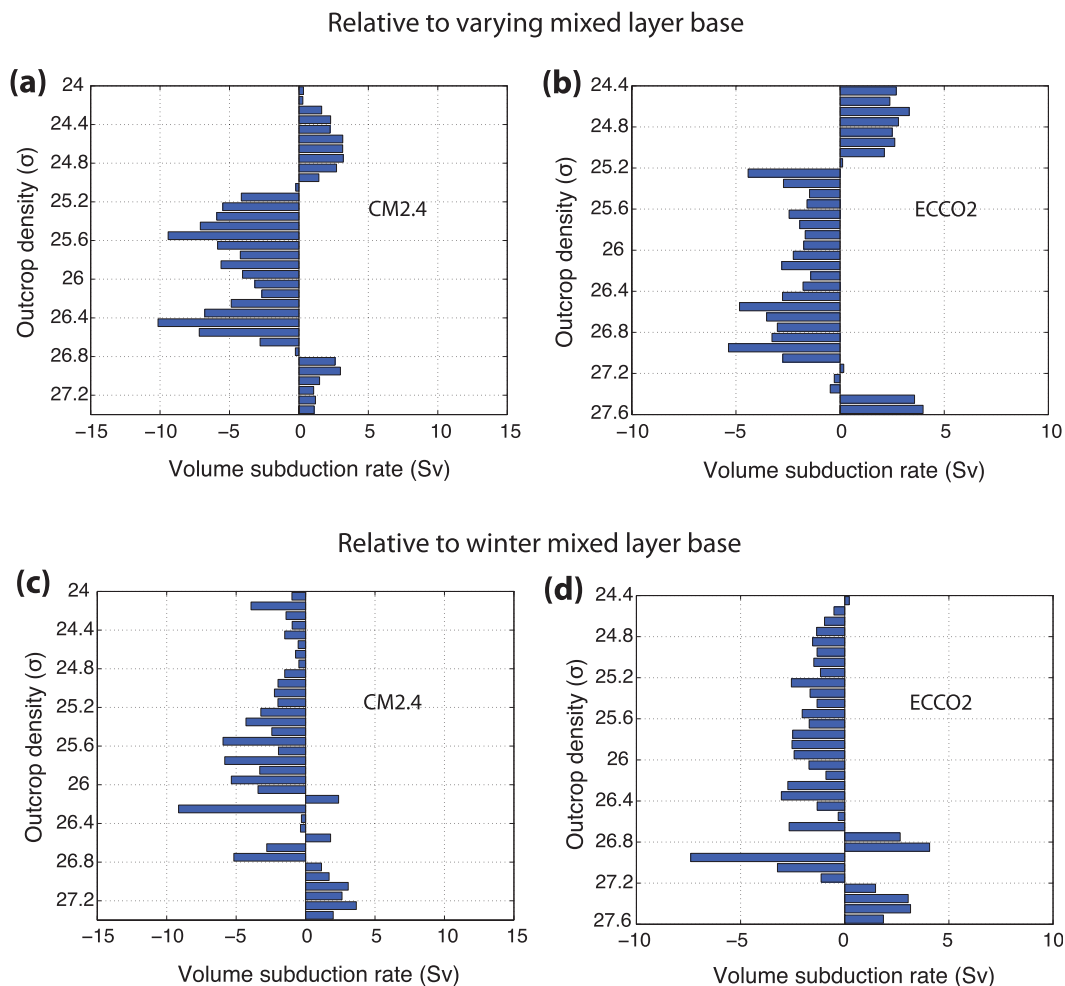## Relative to winter mixed layer base

FIG. 9. A comparison between the volume subduction rates estimated based on two different definitions. (a),(b) The subduction rate is defined as the vertical velocity of water relative to the time-varying mixed layer base (Cushman-Roisin 1987), Eq. (1). (c),(d) The subduction rate is defined as the vertical velocity of water relative to the time-invariant winter mixed layer base (Marshall et al. 1993), Eq. (2). Here, (a) and (c) are computed from the CM2.4 model, and (b) and (d) are computed from the data-constrained ECCO2 product. Monthly climatology fields are used to compute the volume transport in all of the panels. Positive for obduction, negative for subduction. Note the different ranges for the X and Y axes between the CM2.4- and ECCO2-based estimates.

different definitions, and hence indicate the water mass exchange rates across two different control surfaces. While M_H gives us the exchange rate across the time-invariant control surface, which is fixed at the winter mixed layer base, M gives the exchange rate across the base of the mixed layer whose lateral and vertical positions are highly variable in time. The two estimates are subject to differ if diapycnal processes within the seasonal pycnocline modulate the time-mean subduction rate.

We find that the two estimates differ significantly, not only in the mode and intermediate water density range considered thus far, but also in the upper thermocline water masses of $\sigma = 24.0-25.0$ (Figs. 9a and 9c). In the method based on a time-invariant H, the density-

integrated volume flux of the STMW density range ($\sigma = 25.0-26.0$) is about 30% smaller. For the SAMW density class with $\sigma = 26.0-26.8$, the same method yields a density-integrated volume flux that is smaller by 55%. This departure is most pronounced in the SAMW density class where signs of the subduction/obduction are reversed in some density bins between the two estimates. The newly formed water (i.e., the annual mean of the subduction rate across h in a given density) that does not subduct across the winter mixed layer base H in the same density range appears to be diffused into surrounding water masses most of which seems to occur toward the upper-thermocline water density classes of $\sigma = 24.0-25.0$. In this density range (lighter than STMW), the seasonal eddy obduction causes pycnocline
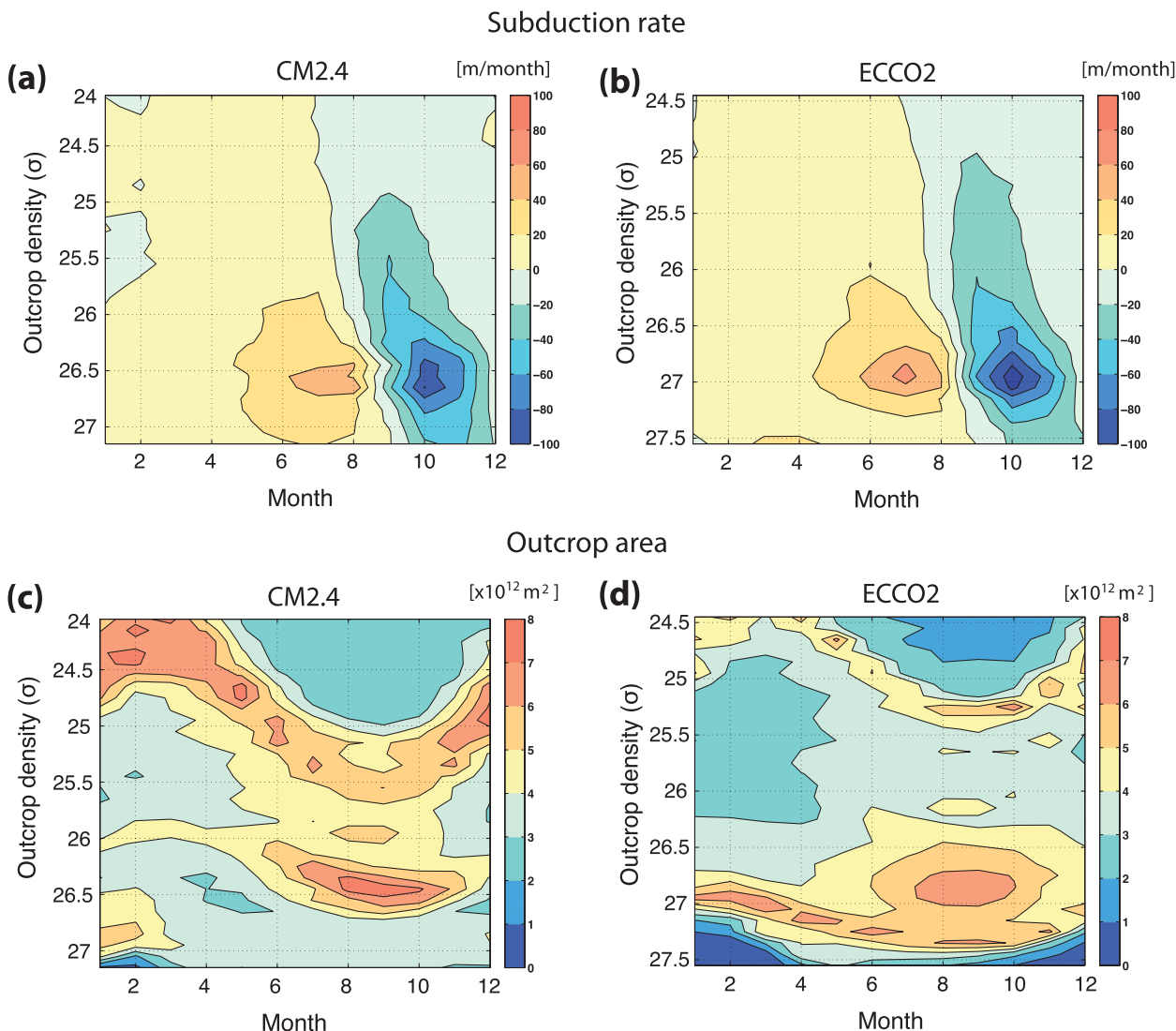
Subduction rate

Outcrop area

FIG. 10. The seasonal cycles of the subduction/obduction rate and the outcrop area. The monthly variations obtained from the CM2.4 model are compared with those obtained from the ECCO2 product. Monthly climatology fields are used to produce the maps. Positive for obduction, negative for subduction. Note that the density range is extended to include lighter waters in (a) and (c), compared to Figs. 6b and 6a.

waters to be entrained into the mixed layer; the outcrop area is greater in summer than in winter (Fig. 10c)—out of phase with the seasonal cycle of the mode water outcrop areas (Fig. 10c). Because an average outcrop area is greater during the obduction period than during the subduction period, the repeating seasonal cycles result in a net obduction volume flux to the mixed layer (Fig. 9a). In contrast to the net obduction across the base of the mixed layer h, the estimate based on a time-invariant H indicates net volume subduction in the density range of $\sigma = 24.0-25.0$ (Fig. 9c). When integrated over the extended density range of $\sigma = 24.0-27.2$, the two subduction rates (i.e., M and M_H) nearly match,

with a total subduction of 53 Sv (1 Sv $\equiv 10^6$ m^3 s^{-1}) below H and a total subduction of 56 Sv below h.

d. Comparison with data-constrained ECCO2 product

The monthly variation and annual mean of the subduction rate obtained from the CM2.4 model are compared with those estimated from the data-constrained Estimating the Circulation and Climate of the Ocean, Phase II (ECCO2) simulation (Menemenlis et al. 2008). To highlight the effect of the seasonal cycle on the time-mean subduction rate, we first compute the monthly climatology fields for density and circulations from the

1993–2009 ECCO2 product and use them to estimate the monthly climatology subduction rate. In this way, we suppress the effects of the interannual variability and meso and submesoscale processes on the estimates of the subduction rates.

The CM2.4-based estimates agree reasonably well with those computed from the ECCO2 product (Figs. 9 and 10). For example, the temporal induction and its seasonal eddy component explain the main mechanism by which mode waters are formed and subducted into the pycnocline (not shown). As is the case for the CM2.4 model, the newly formed mode waters (i.e., waters transferred from the mixed layer to the pycnocline in mode water density classes) exceed the volume of the same density waters subducted into the main pycnocline (Figs. 9b and 9d). The net volume transport relative to varying h is 52 Sv over the mode water density classes of $\sigma = 25.2-27.1$ (Hanawa and Talley 2001), while the net volume transport relative to a winter mixed layer base H is 34 Sv for the same density range. The difference, which accounts for 34% of the newly formed mode waters, appears to be diffused into surrounding water masses within the seasonal pycnocline, particularly toward waters with $\sigma < 25.2$ (Fig. 9b).

The ECCO2-based estimate of the subduction rate into the main pycnocline, 34 Sv over $\sigma = 25.2-27.1$, in turn, agrees reasonably well with previous observationally based estimates of the subduction rate. For example, Sallée et al. (2010) reported about 20 Sv of mode waters subducted into the main pycnocline in a density range of $\sigma = 26.2-27.0$. Our subduction rate is also in accord with the observation-based estimate of meridional transport in the Southern Ocean of 17–18 Sv for $\sigma = 26.5-27.1$ (Cerovečki et al. 2013). On the other hand, our estimate of the mode water formation of 52 Sv is lower than Karstensen and Quadfasel (2002) who reported about 100 Sv of subduction rate using the kinematic approach, 77 Sv of renewal rate using an age tracer, and 87 Sv of formation rate using a thermodynamic approach. Part of the large difference is due to the fact that Karstensen and Quadfasel (2002) considered a wider range of density $\sigma = 23.3-27.3$ for their calculations. A more important reason would be different definitions of the subduction rate inherent in the employed diagnostics.

Notable deficiencies of the CM2.4 model compared to the ECCO2 product include the following: 1) the maximum amplitude of the seasonal cycle in S appears at lighter outcrop densities in the CM2.4 model ($\sigma = \sim26.6$) than in the ECCO2 product ($\sigma = \sim27.0$) (Figs. 10a and 10b) and 2) the CM2.4-simulated subduction rates of upper–Southern Ocean waters, in general, exceed the ECCO2-based estimates. This overestimation is most pronounced in the STMW density class in

association with the exaggerated outcrop areas of STMW in the CM2.4 model (Figs. 10c and 10d). In a study employing the thermodynamic approach of Walin (1982), Speer and Tziperman (1982), and Nurser et al. (1999), Kwon (2013, manuscript submitted to *J. Geophys. Res.*) shows that the CM2.4 model overestimates the transformation and formation rates of the STMW density waters because of the model's misrepresentation of air–sea buoyancy exchange. In the SAMW and AAIW density classes, however, the CM2.4 model captures the observed peaks in the formation and destruction rates of water masses, respectively, consistent with Badin and Williams (2005) and Cerovečki et al. (2013). Overall, the qualitative agreements between the CM2.4 model, the ECCO2 product and previous studies underscore the importance of the seasonal cycle of the upper-ocean dynamics as an essential contributor to the mode water subduction in the Southern Ocean.

5. Conclusions

The role of the seasonal cycle in the subduction rates of upper water masses has previously been discussed in modeling studies based on Lagrangian diagnostics (e.g., Woods 1985; Williams et al. 1995) and in theoretical studies based on thermodynamic approaches (e.g., Marshall et al. 1993; Marshall and Marshall 1995). This study, based on the kinematic approach, agrees with previous studies in suggesting that the main mechanism driving the subduction of mode waters is rapid shoaling of the deep winter mixed layer and the subsequent detrainment of mixed layer waters into the stratified pycnocline in early spring. We further elucidate this mechanism for mode water subduction by showing that the subannual correlations between the temporal change in the mixed layer thickness and the seasonal expansion/contraction of outcrop areas lead to the net annual transport of mixed layer waters into the underlying pycnocline: that is, newly formed mixed layer waters are injected into the pynocline while the winter mixed layer shoals over an expanded outcrop area. This seasonal eddy subduction, along with subduction driven by mesoscale eddies (Marshall 1997), constitutes the dominant mechanism by which Southern Ocean mode waters are formed and transferred to the pycnocline. The seasonal eddy subduction process is most pronounced in SAMW density classes whose winter outcrop positions coincide with the northern flank of the ACC where the mixed layer depths undergo the largest seasonal cycle. The seasonal eddy subduction also plays an important role in determining the net subduction rates of STMW density classes with another important contribution made by Ekman downwelling.

We have shown that the diagnosed subduction rates of upper–Southern Ocean waters differ depending on our choice of the definitions (i.e., across the temporally varying mixed layer base versus across the winter mixed layer base), our choice of models or data products (e.g., the CM2.4 model versus the ECCO2 product), and our choice of temporal resolutions of model solutions (i.e., whether we include the effect of mesoscale eddies or not). They all contribute to the large spread in the subduction rate estimates of upper–Southern Ocean waters, ranging from 6 to 100 Sv (e.g., Sloyan and Rintoul 2001; Karstensen and Quadfasel 2002; Sallée et al. 2010; Cerovečki et al. 2013). In particular, we find that the estimates of the subduction rate based on two different definitions [i.e., the Cushman-Roisin (1987)'s definition based on the varying mixed layer base versus the Marshall et al. (1993)'s definition based on the time-invariant winter mixed layer base] divert significantly over mode water density classes: 40% less transport across the winter mixed layer base in the CM2.4 model and 34% less transport across the winter mixed layer base in the ECCO2 product. This difference can be attributed to diapycnal eddy mixing within the seasonal pycnocline, mainly driven by vertical and lateral diffusive fluxes (Marshall et al. 1999; Nishikawa et al. 2010). Although diapycnal transformation within the seasonal pycnocline highly modulates the volume transport below the seasonal pycnocline, a significant portion of the newly formed mixed layer waters becomes permanently subducted into the main pycnocline. The seasonal eddy subduction is consistent with the Stommel's mixed layer demon that selectively passes the late winter mixed layer waters of low potential vorticity into the underlying pycnocline and subsequently to the main pycnocline.

REFERENCES

Antonov, J. I., and Coauthors, 2010: *Salinity.* Vol. 2, *World Ocean Atlas 2009,* NOAA Atlas NESDIS 69, 184 pp.

Badin, G., and R. G. Williams, 2005: On the buoyancy forcing and residual circulation in the Southern Ocean: The feedback from Ekman and eddy transfer. *J. Phys. Oceanogr.,* **40,** 295–310.

Cerovečki, I., L. D. Talley, M. R. Mazloff, and G. Maze, 2013: Subantarctic mode water formation, destruction and export in the eddy-permitting Southern Ocean State Estimate. *J. Phys. Oceanogr.,* in press.

Cushman-Roisin, B., 1987: Subduction. *Dynamics of the Oceanic Surface Mixed-Layer,* P. Müller and D. Henderson, Eds., Hawaii Institute of Geophysical Special Publications, 181–196.

Da Costa, M. V., H. Mercier, and A. M. Treguier, 2005: Effects of the mixed layer time variability on kinematic subduction rate diagnostics. *J. Phys. Oceanogr.,* **35,** 427–443.

de Boyer Montégut, C., G. Madec, A. S. Fischer, A. Lazar, and D. Iudicone, 2004: Mixed layer depth over the global ocean: An examination of profile data and a profile-based climatology. *J. Geophys. Res.,* **109,** C12003, doi:10.1029/2004JC002378.

Delworth, T. L., and Coauthors, 2006: GFDL CM2 global coupled climate models. Part I: Formulation and simulation characteristics. *J. Climate,* **19,** 643–674.

Dong, S., J. Sprintall, S. T. Gille, and L. Talley, 2008: Southern ocean mixed-layer depth from Argo float profiles. *J. Geophys. Res.,* **113,** C06013, doi:10.1029/2006JC004051.

Downes, S. M., A. S. Budnick, J. L. Sarmiento, and R. Farneti, 2011: Impacts of wind stress on the Antarctic circumpolar current fronts and associated subduction. *Geophys. Res. Lett.,* **38,** L11605, doi:10.1029/2011GL047668.

Farneti, R., and T. L. Delworth, 2010: The role of mesoscale eddies in the remote oceanic response to altered Southern Hemisphere winds. *J. Phys. Oceanogr.,* **40,** 2348–2354.

——, ——, A. J. Rosati, S. M. Griffies, and F. Zeng, 2010: The role of mesoscale eddies in the rectification of the Southern Ocean response to climate change. *J. Phys. Oceanogr.,* **40,** 1539–1557.

Follows, M. J., and J. C. Marshall, 1994: Eddy-driven exchange at ocean fronts. *Ocean Modell.,* **102,** 5–9.

Griffies, S. M., 2009: Elements of MOM4P1. GFDL Ocean Group Tech. Rep. 6, 444 pp.

Hanawa, K., and L. D. Talley, 2001: Mode waters. *Ocean Circulation and Climate,* G. Siedler, J. Church, and J. Gould, Eds., Academic, 373–386.

Hazeleger, W., and S. S. Drijfhout, 2000: Eddy subduction in a model of the subtropical gyre. *J. Phys. Oceanogr.,* **30,** 677–695.

Iselin, C. O. D., 1939: The influence of vertical and lateral turbulence on the characteristics of waters at mid-depth. *Trans. Amer. Geophys. Union,* **20,** 414–417.

Karstensen, J., and D. Quadfasel, 2002: Formation of southern hemisphere pycnocline waters: Water mass conversion and subduction. *J. Phys. Oceanogr.,* **32,** 3020–3038.

Koch-Larrouy, A., R. Morrow, T. Penduff, and M. Juzal, 2010: Origin and mechanism of Subantarctic Mode Water formation and transformation in the southern Indian Ocean. *Ocean Dyn.,* **3,** 563–583, doi:10.1007/s10236-010-0276-4.

Locarnini, R. A., A. V. Mishonov, J. I. Antonov, T. P. Boyer, H. E. Garcia, O. K. Baranova, M. M. Zweng, and D. R. Johnson, 2010: *Temperature.* Vol. 1, *World Ocean Atlas 2009,* NOAA Atlas NESDIS 69, 184 pp.

Marshall, D., 1997: Subduction of water masses in an eddying ocean. *J. Mar. Res.,* **55,** 201–222.

——, and J. C. Marshall, 1995: On the thermodynamics of subduction. *J. Phys. Oceanogr.,* **25,** 138–151.

Marshall, J. C., and T. Radko, 2003: Residual-mean solutions for the Antarctic circumpolar current and its associated overturning circulation. *J. Phys. Oceanogr.,* **33,** 2341–2354.

——, R. G. Williams, and A. J. G. Nurser, 1993: Inferring the subduction rate and period over the North Atlantic. *J. Phys. Oceanogr.,* **23,** 1315–1329.

——, D. Jamous, and J. Nilsson, 1999: Reconciling thermodynamic and dynamic methods of computation of water-mass transformation rates. *Deep-Sea Res. I,* **46,** 545–572.

McCartney, M. S., 1977: Subantarctic mode water. *Deep-Sea Res.,* **24,** 103–119.

Menemenlis, D., J. M. Campin, P. Heimbach, C. Hill, T. Lee, A. Nguyen, M. Schodlock, and H. Zhang, 2008: ECCO2: High resolution global ocean and sea ice data synthesis. *Mercator Ocean Quarterly Newsletter,* No. 31, Mercator Ocean, Ramonville-Saint-Agne, France, 13–21.

Nishikawa, S., H. Tsujino, K. Sakamoto, and H. Nakano, 2010: Effects of mesoscale eddies on subduction and distribution of subtropical mode water in an eddy-resolving OGCM of the western North Pacific. *J. Phys. Oceanogr.,* **40,** 1748–1765.

Nurser, A. J. G., and J. C. Marshall, 1991: On the relationship between subduction rates and diabatic forcing of the mixed layer. *J. Phys. Oceanogr.,* **21,** 1793–1802.

——, R. Marsh, and R. G. Williams, 1999: Diagnosing water mass formation from air–sea fluxes and surface mixing. *J. Phys. Oceanogr.,* **29,** 1468–1487.

Qiu, B., and R. X. Huang, 1995: Ventilation of the North Atlantic and North Pacific: Subduction versus obduction. *J. Phys. Oceanogr.,* **25,** 2374–2390.

Reynolds, R. W., N. Rayner, T. M. Smith, D. Stokes, and W. Wang, 2002: An improved in situ and satellite SST analysis for climate. *J. Climate,* **15,** 1609–1625.

Sabine, C. L., and Coauthors, 2004: The oceanic sink for anthropogenic CO_2. *Science,* **305,** 367–371.

Sallée, J.-B., K. Speer, S. Rintoul, and S. Wijffels, 2010: Southern ocean thermocline ventilation. *J. Phys. Oceanogr.,* **40,** 509–529.

Sarmiento, J. L., N. Gruber, M. A. Brzezinski, and J. P. Dunne, 2004: High-latitude controls of pycnocline nutrients and low latitude biological productivity. *Nature,* **427,** 56–60.

Sloyan, B. M., and S. R. Rintoul, 2001: Circulation, renewal, and modification of Antarctic mode and intermediate water. *J. Phys. Oceanogr.,* **31,** 1005–1030.

Speer, K., and E. Tziperman, 1982: Rates of water mass formation in the North Atlantic Ocean. *J. Phys. Oceanogr.,* **22,** 93–104.

Stommel, H., 1979: Determination of water mass properties of water pumped down from the Ekman layer to the geostrophic flow below. *Proc. Natl. Acad. Sci. USA,* **76,** 3051–3055.

Toggweiler, J. R., K. Dixon, and K. Bryan, 1989: Simulations of radiocarbon in a coarse-resolution world ocean model 2. Distributions of bomb-produced carbon 14. *J. Geophys. Res.,* **94,** 8243–8264.

Walin, G., 1982: On the relation between sea-surface heat flow and thermal circulation in the ocean. *Tellus,* **34,** 187–195.

Williams, R. G., J. C. Marshall, and M. A. Spall, 1995: Does Stommel's mixed layer ''demon'' work? *J. Phys. Oceanogr.,* **25,** 3089–3102.

Woods, J. D., 1985: Physics of thermocline ventilation. *Coupled Atmosphere–Ocean Models,* J. C. J. Nihoul, Ed., Elsevier, 543–590.